Materials Today Sustainability 29 (2025) 101059

Contents lists available at ScienceDirect

Materials Today Sustainability

journal homepage: www.journals.elsevier.com/materials-today-sustainability

Phytofabrication of silver nanoparticles using *Ehretia rigida* leaf aqueous extract, their characterization, antioxidant and antimicrobial activities

Samson O. Oselusi [a,b], Nicole R.S. Sibuyi [b,c], Mervin Meyer [b], Samantha Meyer [d], Abram M. Madiehe [a,b,*]

[a] Nanobiotechnology Research Group, Department of Biotechnology, University of the Western Cape, Private Bag X17, Bellville, Cape Town, 7535, South Africa
[b] DSI/Mintek Nanotechnology Innovation Centre, Biolabels Node, Department of Biotechnology, University of the Western Cape, Private Bag X17, Bellville, Cape Town, 7535, South Africa
[c] Health Platform, Advanced Materials Division, Mintek, 200 Malibongwe Drive, Randburg, 2125, South Africa
[d] Phytotherapy Research Group, Department of Biomedical Sciences, Cape Peninsula University of Technology, P.O. Box 1906, Bellville, 7535, South Africa

ARTICLE INFO

Keywords:
Ehretia rigida
Silver nanoparticles
Green synthesis
Antioxidant activity
Antimicrobial activity

ABSTRACT

The green synthesis of nanoparticles (NPs) offers a sustainable, rapid, and cost-effective alternative to traditional chemical and physical methods, with diverse applications across various fields. This study reports the synthesis of silver nanoparticles (AgNPs) using *Ehretia rigida* (Er) leaf aqueous extract and evaluates their biological activities. The formation of the NPs was confirmed by the change in colour from clear to dark brown. The synthesis parameters, such as pH, temperature, Er extract and silver nitrate ($AgNO_3$) concentrations, reaction ratio, and incubation time, were optimized for high yields, controlled size, and stability of the NPs. The optimized Er-AgNPs were characterized using ultraviolet–visible (UV–vis) spectroscopy, dynamic light scattering (DLS), Fourier transform infrared (FTIR) spectroscopy, and high-resolution transmission electron microscopy (HR–TEM). The Er-AgNPs sample presented a characteristic absorbance peak at 408 nm, a hydrodynamic size of 74.02 ± 0.19 nm, a polydispersity index (PDI) of 0.39 ± 0.05, and a zeta potential of −25.4 ± 6.26 mV. FTIR analysis revealed the nature of the biomolecules responsible for the reduction and stabilization of the NPs. HR–TEM revealed that the Er-AgNPs were spherical, with core sizes ranging from 6 to 18 nm. The Er leaf aqueous extract and Er-AgNPs possessed antioxidant activities, with the Er leaf extract having higher activity than Er-AgNPs. The Er leaf extract did not exhibit any antimicrobial activity, whereas the Er-AgNPs demonstrated broad-spectrum antimicrobial activities against all the tested pathogens. This study provides a sustainable, easy and cost-effective method to produce AgNPs for biomedical applications.

1. Introduction

Metal-based nanoparticles (MNPs) have gained increasing attention in materials science because of their unique morphology, size distribution, and optical, magnetic, and biological properties, which are different from those of bulk metals [1,2]. These exceptional and multifaceted properties have driven extensive research and development in multidisciplinary fields such as biotechnology, medicine, agriculture, electronics, energy, and environmental science [2–4]. Metals, including gold, silver, platinum, palladium, iron, copper, zinc, and titanium, are integral to the synthesis and application of various MNPs. In particular, AgNPs have garnered significant attention because of their remarkable physicochemical properties, which include a large surface-area-to-volume ratio, high reactivity, and electrical conductivity [5]. AgNPs are invaluable in diverse applications, especially in agriculture, medicine, water purification, pharmaceutics, catalysis, and bio-labelling [6–10]. In agriculture, AgNPs have been used to increase crop growth and overall agricultural sustainability by acting as nano-fertilizers or nano-pesticides and by protecting crops against plant pathogens [11]. Their biomedical applications include the development of cutting-edge antimicrobial agents, materials for tissue restoration and regeneration, drug delivery formulations, detection and diagnosis platforms, and performance-enhanced treatment alternatives [10].

Currently, researchers are actively investigating the full potential of

* Corresponding author. Nanobiotechnology Research Group, Department of Biotechnology, University of the Western Cape, Private Bag X17, Bellville, Cape Town, 7535, South Africa.
E-mail address: amadiehe@uwc.ac.za (A.M. Madiehe).

https://doi.org/10.1016/j.mtsust.2024.101059
Received 2 October 2024; Received in revised form 20 November 2024; Accepted 8 December 2024
Available online 9 December 2024

AgNPs through innovative synthesis methods and functionalization techniques to improve their efficiency, specificity and safety. For example, a variety of physical (laser ablation, thermal evaporation, etc.) and chemical (chemical reduction, sol-gel, chemical vapour decomposition, hydrothermal fabrication, etc.) techniques have been used in the synthesis of AgNPs [3,4,12,13]. While most of these methods provide the benefit of bulk synthesis with good control of the particle size distribution, the use of costly and hazardous materials, extreme reaction conditions, and non-biocompatibility of the resulting NPs limit their applications [1–3,14]. Consequently, green chemistry has shifted the interest of researchers toward the search for non-toxic, eco-friendly, and cost-effective approaches to fabricate nanomaterials [3,15].

The green chemistry approach is characterized by high versatility, energy efficiency, reproducibility, and the use of non-toxic materials [16]. Although microorganisms resources can offer viable and eco-friendly alternatives to traditional synthesis, plant extracts are often preferred because of their simplicity, ease of handling, scalability, chemical diversity, and cost-effectiveness [14,15]. Additionally, plant extracts can be obtained from multiple parts, including the stem, root, latex, fruits, seeds, leaves, flowers, agro-waste, peels, and bark [15,17,18]. These benefits make plant extract-based synthesis of NPs more attractive, particularly in large-scale production for agricultural and biomedical applications of MNPs.

Various extracts have been used as reducing or capping agents in the synthesis of AgNPs for different applications. For example, AgNPs synthesized from the leaf extract of *Cymbopogon citratus* have proven to be potent sources of antioxidants and have demonstrated antibacterial activity against drug-resistant pathogens such as *Bacillus cereus*, *Enterococcus faecalis*, *Escherichia coli*, and *Shigella flexneri* [1]. Similarly, the synthesis of AgNPs using aqueous extracts of *Sanvitalia procumbens* [12], *Euphorbia rigida* [19], *Acalypha indica* [20] and *Clinacanthus nutans* [21] has been reported to involve an abundance of phytoconstituents that aid in the fabrication of AgNPs, which have been exploited for other applications, such as the photocatalytic degradation of dyes and anticancer studies. Some of these phytoconstituents, including flavonoids, ketones, aldehydes, terpenoids, tannins, carbohydrates, and phenolic acids, have been implicated in the reduction of Ag^{+} to Ag^{0} during the synthesis and stabilization of AgNPs [20,22,23].

E. rigida, also known as puzzle bush, is a deciduous shrub or small tree belonging to the Boraginaceae family and is native to Southern Africa, particularly in regions such as South Africa, Botswana, and Namibia, where it is valued for its medicinal properties [24]. Traditional healers in these regions use the leaves of this plant for anti-inflammatory, antimicrobial, and antioxidant activities and as natural remedies against a wide range of diseases. These activities highlight its importance in ethnomedicine [24]. As part of an attempt to unlock all the benefits and integrate their use into modern medicine, Shukla et al. [25] systematically explored the pharmacological potential of the *Ehretia* genus. The authors reported that the crude extracts or individual compounds from the genus presented antioxidant, anti-inflammatory, antibacterial, antitubercular, antiallergic, and anti-snake venom activities. In another study, phytoconstituents from Ehretia species were isolated and characterized to identify the compounds responsible for their medicinal properties [26]. Furthermore, a recent publication from our research group investigated the antimicrobial activities of some of these phytoconstituents against *Klebsiella pneumoniae* carbapenemase at the molecular level [27]. However, there is still a paucity of information regarding the use of *Ehretia rigida* in green nanotechnology. Driven by the pressing public health challenges of multidrug-resistant pathogens and the potential of green nanotechnology, the present study was undertaken to synthesize AgNPs from *E. rigida* leaves. The synthesized Er-AgNPs were confirmed by UV–vis spectroscopy and characterized via DLS and HR–TEM. The potential biological applications of Er leaf aqueous extract and Er-AgNPs were subsequently tested through antioxidant and antibacterial assays.

2. Methodology

2.1. Plant selection, identification, and collection

The plant *E. rigida* was selected for the present study based on available knowledge of its traditional medicinal use. The leaves of the plant *E. rigida* (identification number; 175/69) were collected in June at the Kirstenbosch National Botanical Garden (South African National Biodiversity Institute, Cape Town, South Africa). The leaves were transported immediately to the Nanobiotechnology Research Laboratory (Department of Biotechnology, University of the Western Cape) for further studies.

2.2. Preparation of extracts

The *E. rigida* plant leaves were thoroughly washed under running tap water, rinsed with distilled water, and oven-dried at 70 °C for 3 days. The dried leaves were ground to a fine powder using a coffee grinder and stored in airtight plastic bags until further use. The protocols described by Dube et al. [28] were adapted for the aqueous extraction of Er leaf powder. Briefly, 40 g of leaf powder was mixed with 400 ml of deionized water (ddH_2O) in a 1000 ml Erlenmeyer flask. The mixture was heated in a microwave for 5 min and then stirred for 24 h at room temperature. Thereafter, the sample was centrifuged on a Sorvall Lynx 6000 superspeed centrifuge (Thermo Fisher Scientific, Massachusetts, USA) at 9000 rpm for 10 min at room temperature. The supernatant was vacuum filtered with Whatman No. 1 filter paper and further microfiltered with a 0.45 μm filter to remove residual plant material. The sample was then frozen overnight at −80 °C and subsequently freeze-dried (SP Scientific Pennsylvania, USA) at −53 °C to obtain the dried aqueous extract. The percentage yield of the powdered aqueous extract was determined, and the sample was kept in a desiccator for later use.

2.3. Synthesis of Er-AgNPs

The synthesis of AgNPs was performed by reducing $AgNO_3$ with the Er leaf aqueous extract. To this end, the crude extract was dissolved in ddH_2O to yield a 125 mg/ml stock solution. A preliminary experiment was performed, where 1 mM $AgNO_3$ was preheated on a thermomixer (Eppendorf, Hamburg, Germany) to 90 °C for 5 min, and an aliquot of 12.5 mg/ml extract was added at a 1:9 v/v ratio to a final volume of 400 μl. The mixture was then incubated at 750 rpm for 1 h at 90 °C in the dark.

2.3.1. Optimization of the synthesis of Er-AgNPs

The effects of various parameters, which include temperature, pH, Er leaf extract concentration, $AgNO_3$ concentration, the ratio of leaf extract to $AgNO_3$, and incubation time, on the synthesis of Er-AgNPs, were evaluated to determine the optimal conditions required to produce AgNPs. The effect of temperature was studied by incubating a mixture of $AgNO_3$ and extract on a thermomixer at temperatures ranging from 25 to 90 °C. For pH, the natural pH of the extract was determined and thereafter adjusted to different pH values ranging from 3 to 11 prior to synthesis. The extract concentration was optimized to range from 1.56 to 100 mg/ml, and the $AgNO_3$ concentration ranged from 0.5 to 5 mM. The effect of the leaf extract to $AgNO_3$ ratio on the spectrum transition was determined by increasing the volume of $AgNO_3$ in the solution against the Er leaf extract to ratios of 1:1, 1:3, 1:5, 1:7, and 1:9. The effect of incubation time on the synthesis of Er-AgNPs was determined by recording the changes in the SPR peaks and maximum absorbance at different time intervals between 0 min and 8 h while keeping all optimized parameters constant. All reactions were subjected to centrifugation at 16,000 rpm for 45 min at room temperature and thereafter washed two times with ddH_2O. The absorption spectra of the samples were subsequently measured at 300–800 nm using a POLARstar Omega microplate reader (BMG LABTECH, Offenberg, Germany). Finally, Er-

AgNPs synthesis was scaled up to 30 ml following the optimum conditions and was used for further studies.

2.3.2. Characterization of Er-AgNPs

Characterization of Er-AgNPs was performed using the methods described in previous studies [28,29]. A DLS Zetasizer (Nano-ZS; Malvern Instruments, UK) was used to determine the hydrodynamic size, size distribution, PDI, and zeta (ζ) potential at 25 °C and a 90° angle. To measure the hydrodynamic size and PDI, the Er-AgNPs were diluted with ddH2O at a 1:10 (v/v) ratio and transferred into a 10 mm square polystyrene cuvette. Similarly, for the ζ measurements, 800 μl of the diluted sample was loaded into a disposable folded capillary cell and analysed at a voltage of 4 mV. The FTIR data of the leaf extract and Er-AgNPs were determined in the wavenumber range of 4000 cm^{-1}–400 cm^{-1} using a PerkinElmer Spectrum Two Spectrometer FTIR instrument (Waltham, MA, USA). The dried samples were mixed with potassium bromide (KBr) powder and pressed into a round disk. A pure KBr disk was used for background correction. The spectra were then analysed via OriginPro 8.5 software (OriginLab Corporation, Massachusetts, USA). The detailed core size and morphology of the Er-AgNPs were determined via HR–TEM (Thermo Fisher Scientific, Massachusetts, USA). One drop of an ultrasonically dispersed sample was placed on a carbon-coated copper grid via the drop-coating method [30]. The sample was then analysed on an FEI Tecnai G2 20 field-emission gun operated in bright field mode at an accelerating voltage of 200 kV. Finally, the micrograph images obtained from the HR–TEM analysis were used to estimate the core size of the Er-AgNPs via ImageJ software (National Institute of Health, USA) and OriginPro 8 SR4 software (V8.0951).

2.3.3. In vitro stability test

The *in vitro* stability of the Er-AgNPs in selected biological media was assessed according to previous studies [28,31] with slight modifications. This study was carried out by diluting a stock suspension of Er-AgNPs with Müeller–Hinton broth (MHB) or ddH_2O at a 1:1 ratio to a final volume of 1 ml. The mixture was incubated at 37 °C, and the UV–vis absorbance was recorded at different intervals for 24 h.

2.4. Quantitative phytochemical and total antioxidant capacity

2.4.1. Total phenolic content (TPC)

Phenolic compounds are integral plant components that contain hydroxyl groups that are responsible for facilitating free radical scavenging activities [32]. The TPC in the Er leaf extract and Er-AgNPs were determined via a slight modification to the Folin−Ciocalteu spectrophotometric method described by Kocazorbaz [19] and Singh et al. [33]. Overall, the reaction was carried out by mixing 100 μl of the test samples at 800 μg/ml with 1 ml of 10 % Folin–Ciocalteu reagent, and the mixture was incubated for 5 min at room temperature in the dark. Subsequently, 800 μl of sodium carbonate (Na_2CO_3, 7.5 %) was added, and the mixture was further incubated for 60 min. The absorbance of the solutions was read at 760 nm against a blank reagent (samples replaced with ddH_2O) using a UV–vis spectrophotometer. Gallic acid (0–400 μg/ml) dissolved in methanol was used as a standard to obtain the calibration curve. The total phenolic content was determined as mg of gallic acid equivalents (GAE) per gram of dried sample.

2.4.2. Total flavonoid content (TFC)

The TFC of the Er leaf extract and Er-AgNPs was estimated via the aluminium chloride method reported by Mat et al. [21], with slight modifications. The reaction consisted of 25 μl of the samples at a concentration of 800 μg/ml, 125 μl of ddH_2O, and 7.5 μl of $NaNO_3$ (5 % w/v). The mixture was incubated at room temperature for 5 min. Subsequently, 15 μl of $AlCl_3$ (10 % w/v) solution was added to the mixture, which was left at room temperature for 6 min before 50 μl of 1 M NaOH and 27.5 μl of ddH2O were added. The mixture was incubated in the dark for 20 min, and the absorbance was measured at 510 nm. The TFC was expressed as mg quercetin (QE) per gram of dried extract using quercetin as a standard curve.

2.4.3. 1,1 diphenyl-2-picrylhydrazyl (DPPH) assay

The free radical scavenging potential of the Er leaf extract and Er-AgNPs was determined by measuring the radical scavenging activity of DPPH, as described by Maungchanburee et al. [34], with slight modifications. A 0.3 mM DPPH solution was prepared by dissolving 5.9 mg of DPPH in 50 ml of methanol. The mixture was covered with aluminium foil and homogenized in an ultrasonic water bath for 30 s. Aliquots (100 μl) of different concentrations of the test samples (6.25–100 μg/ml) were mixed with the DPPH solution at a 1:1 ratio in a 96-well plate. The mixture was incubated at room temperature in the dark for 30 min. Ascorbic acid (AA) was used as the standard, and methanol was used as a negative control. After incubation, the residual absorbance of the DPPH radical was measured at 517 nm, and the free radical scavenging potency (% scavenging activity) was calculated via the following formula:

$$\%\ \text{Antioxidant activity} = \frac{(A1 - A2)}{A1} \times 100$$

where:

A1 = the absorbance of the negative control, and A2 = the absorbance of the test sample.

2.4.4. ABTS (2,2-azino-bis (3-ethylbenzthiazoline-6-sulphonic acid)) radical scavenging assay

The ABTS radical scavenging activity of the Er extract and AgNPs was determined according to a previously described method [35,36], with slight modifications. The ABTS free radical was obtained by mixing an equal volume of 2.45 mM $K_2S_2O_8$ and 7.4 mM ABTS stock solution and incubating it in the dark for 16 h at room temperature. The absorbance (at 734 nm) of the mixture was then adjusted to 0.700 ± 0.02 by adding methanol to obtain the working solution. The antioxidant activity was measured by mixing 20 μl of test samples at different concentrations (6.25–100 μg/ml) with the ABTS working solution at a ratio of 1:9 in a 96-well plate. After incubating the sample in the dark for 15 min, the absorbance was measured at 734 nm using a plate reader. AA was used as the positive control, and methanol was used as the negative control. Finally, the percentage of inhibition of radicals was determined using the following formula:

$$\%\ \text{inhibition} = \frac{(A1 - A2)}{A1} \times 100$$

where:

A1 = the absorbance of the negative control (ABTS radical + methanol), and A2 = the absorbance of the test samples/standard.

2.4.5. Ferric-reducing antioxidant power (FRAP) assay

The FRAP of the Er extract and AgNPs was determined using an assay described previously [37], with slight modifications. Fresh FRAP reagent was prepared by mixing 300 mM acetate buffer (pH 3.6), 10 mM 2, 4,6-tris(2-pyridyl)-*s*-triazine, and 20 mM ferric chloride solutions at a 10:1:1 (v/v/v) ratio. The mixture was kept in the dark for 30 min. The FRAP activity was measured by mixing 10 μl of test samples at different concentrations (12.5–400 μg/ml) with 300 μl of FRAP reagent thoroughly in a 96-well plate. After incubating the sample for 30 min in the dark, the absorbance was read at 593 nm using a microplate reader. The reagent blank (FRAP reagent + distilled water) and AA were used as negative and positive controls, respectively. An aqueous solution of $FeSO_4$ was used to generate a standard curve. The FRAP activity was presented as the ferrous (Fe^{2+}) equivalent in μM.

2.5. Antimicrobial effects of the leaf extract and Er-AgNPs

2.5.1. Microbial strains and culture

The antimicrobial effects of Er leaf extract and Er-AgNPs were tested against eight bacterial strains: *Staphylococcus aureus,* methicillin-resistant *Staphylococcus aureus*, *Streptococcus pyogenes, Acinetobacter baumannii, Escherichia coli*, *Enterobacter cloacae, Klebsiella pneumoniae*, *Pseudomonas aeruginosa*, and one fungal strain, *Candida albicans*. MacFarland's turbidity standard was used for the standardization of the antimicrobial susceptibility tests following the method outlined by Balouiri et al. [38] with slight modifications. Briefly, each of the bacterial strains was streaked onto Müeller–Hinton agar (MHA, Sigma–Aldrich) and incubated at 37 °C for 24 h. Similarly, the fungus was streaked on potato dextrose agar (PDA, Sigma–Aldrich) and incubated at 37 °C for 48 h. Thereafter, single colonies from the different cultures were inoculated in 2 ml of their respective broths and incubated for 1 h at 37 °C in a shaking incubator set at 200 rpm. The bacterial cultures were adjusted to 0.5 McFarland standard corresponding to an OD_{600} of 0.08–0.1.

2.5.2. Antimicrobial effects of Er leaf extract and Er-AgNPs determined using agar well diffusion assay

The antimicrobial test was carried out using the agar well diffusion method according to the Clinical & Laboratory Standards Institute for bacteria and yeast testing [38]. Using sterile cotton swabs, the selected bacterial and yeast suspensions at 0.5 McFarland turbidity standard were evenly spread on MHA and PDA plates, respectively. Thereafter, 4 mm diameter wells were prepared on the plates using the blunt end of sterile 200 µl micropipette tips. Subsequently, 50 µl of the extract (800 µg/ml), Er-AgNPs (800 µg/ml), positive controls (ciprofloxacin and amphotericin-B; 10 µg/ml), and negative control (broth) were added to the respective wells. The plates were left at room temperature for 30 min and then incubated at 37 °C for 24 h for bacterial and 48 h for yeast samples. After incubation, the antimicrobial activities of the test samples were assessed by observing the formation of clear zones of inhibition (ZOIs) around the wells. The clear zones were measured in millimetres using a Vernier calliper.

2.5.3. Antimicrobial effects of Er-AgNPs using a micro broth dilution assay

The Er-AgNPs that showed antimicrobial activity in the agar well diffusion assay were subjected to a micro broth dilution assay as described in previous studies [38,39]. The bacterial inoculums in MHB and fungi in potato dextrose broth (PDB) were standardized to 0.5 MacFarland. At a density of 10^6 CFU/ml, 50 µl aliquots of each of the microbes were added to equal amounts of twofold dilutions of the samples in their respective broths in 96-well microtiter plates. After mixing, the inoculated plates were incubated at 37 °C for 24 h for bacterial and 48 h for yeast samples. The wells were visually examined for the absence of microbial growth/turbidity, and the lowest concentration which resulted in growth inhibition was identified as the minimum inhibitory concentration (MIC). This was further verified by measuring the absorbance of the suspension spectrophotometrically at OD_{600}. The same process was used to determine the MICs for ciprofloxacin and amphotericin-B, which were used as positive controls for bacterial and fungal cultures, respectively.

2.5.4. Determination of the minimum bactericidal/fungicidal concentration

The minimum bactericidal and minimum fungicidal concentrations (MBC and MFC) were determined using the methods described by Loo et al. [39] and Mackeen et al. [40], with slight modifications. A loopful of the wells that showed no visible bacterial growth were seeded on their respective agar plates and further incubated as described above for bacteria and yeast. The lowest concentration of Er-AgNPs or positive control that resulted in no growth on the plate was recorded as the MBC/MFC.

2.6. Statistical analysis

All data were analysed statistically using GraphPad Prism software, version 8.0.1 (GraphPad Software Inc., San Diego, CA). The descriptive data were expressed as mean ± standard error of the mean (SEM) or standard deviation (SD), and statistical variations were determined using one way analysis of variance (ANOVA). The differences were considered statistically significant when $p < 0.05$.

3. Results and discussion

3.1. Plant extraction and Er-AgNPs synthesis

The Er leaf aqueous extract was obtained using microwave-assisted macerationafter which the samples were stirred for 24 h at room temperature. to ensure complete extraction. Maceration techniques are preferred for extraction to sustain the presence of heat-labile compounds, which can be altered or degraded when heating is performed for a long period [41]. Aqueous extraction is preferred because of its significant advantages in terms of accessibility, safety, efficacy, and percentage yield [21,42]. The percentage yield of the extraction of Er leaf extract powder was 12.96 %.

A synthesis reaction at 90 °C using a mixture of 12.5 mg/ml Er leaf aqueous extract and 1 mM $AgNO_3$ solution at a ratio of 1:9 produced a visual colour change from clear to dark brown (Fig. 1a), indicating the formation of AgNPs during the reaction. This was further confirmed by the presence of an SPR peak at approximately 402 nm (Fig. 1b).

One of the primary and most fascinating characteristics of MNPs is their optical properties, which change proportionately with size and shape [12]. In the present study, the Er leaf extract and $AgNO_3$ solution did not present an absorbance peak in the visible region (Fig. 1b). However, incubation of a mixture of $AgNO_3$ and Er leaf aqueous extract at 90 °C resulted in absorption spectra in the wavelength range of 300–700 nm. The formation of an SPR peak at 402 nm indicated the presence of Er-AgNPs in the aqueous colloidal solution. This is due to the abundance of phytochemicals present in the leaf extract, which act as either reducing or capping agents or both and aid in the biosynthesis of AgNPs [5]. This observation is consistent with those reported in the literature, where a colour change in the reaction mixture between the $AgNO_3$ solution and plant extracts resulted in the formation of AgNPs [12,43]. Other studies have also established that the SPR band for AgNPs occurs in the range between 400 and 450 nm [44,45] due to the excitation of surface plasmon vibrations [46].

3.2. Optimization of Er-AgNPs synthesis

Different parameters, such as temperature, pH, Er leaf extract and $AgNO_3$ concentrations, and reaction time, have been shown to have direct effects on the crystallinity, size, shape, and dispersity of MNPs [32,47]. As a result, the effects of these parameters on the synthesis of Er-AgNPs were investigated via UV–vis, in which one variable was changed at a time.

3.2.1. Effects of the reaction temperature on Er-AgNPs biosynthesis

Optimization of the reaction temperature was performed by synthesising the Er-AgNPs at different temperatures and monitoring changes in UV–vis spectroscopy for each reaction after 1 h. As shown in Fig. 2a, the SPR peaks of Er-AgNPs synthesized at 25 °C with or without shaking (static) were characterized by the appearance of a shoulder, which may imply that various sizes and shapes of Er-AgNPs were formed. Above 25 °C, Er-AgNPs with symmetrical and narrow SPR peaks were observed, resulting in efficient and optimal production at 50 °C. A further increase in the reaction temperature (up to 90 °C) resulted in a corresponding decrease in the absorbance intensity, which indicated the formation of fewer Er-AgNPs. Therefore, 50 °C was selected as the optimum temperature for Er-AgNPs synthesis. This study corroborates

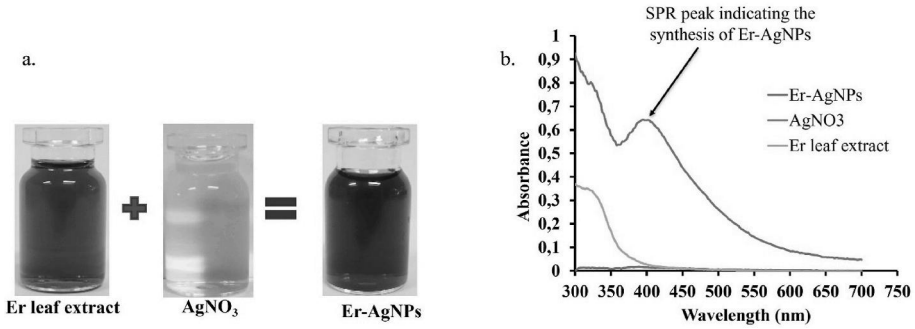

Fig. 1. Er leaf aqueous extract. (a) Visual observation of colour change indicating the synthesized Er-AgNPs, and (b) UV–vis spectra of the Er leaf extract and Er-AgNPs. The change in colour to dark brown was characterized by the presence of an SPR peak at 402 nm, which indicated the production of Er-AgNPs.

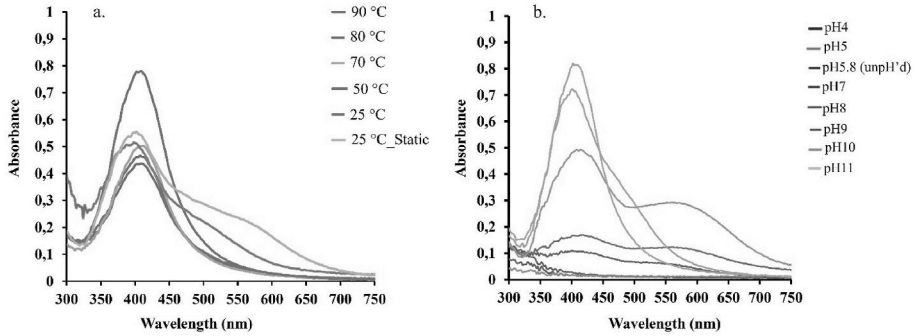

Fig. 2. UV–vis spectra showing the effects of varying temperatures (a) and pH values (b) on the synthesis of Er-AgNPs.

findings from AgNPs synthesis using *Zingiber officinale* root extract [48] and *Saussurea costus* [49], both of which achieved an optimum reaction temperature of 50 °C and produced uniform-sized AgNPs. *Salvia africana–Lutea* [28] and *Azadirachta indica* [50] leaf extracts established an optimum reaction temperature of 70 °C for plant extract-mediated AgNPs production. In addition, *Aloe fleurentinorum* leaf extracts [51], *Euclayptus cameldulensis* leaf extracts, and *Terminalia arjuna* bark extracts [20] have been reported to synthesize AgNPs at optimum reaction temperatures of 60 and 75 °C, respectively. Other studies have shown that higher reaction temperatures can lead to smaller-sized AgNPs [52], whereas excessively high temperatures can result in adverse effects, such as the decomposition of reducing agents in the extracts or changes in the morphology and stability of the MNPs [52,53].

3.2.2. *Effects of pH on Er-AgNPs biosynthesis*

pH is a crucial parameter that influences the stability, size, and morphology of NPs [54,55]. This is due to its ability to change the charge of biomolecules, affecting their capping and stabilizing abilities. In this study, the natural pH (unpH'd) of the extract was established to be 5.8, which was further adjusted to various pH values ranging from 3 to 11 using 0.1 M NaOH to achieve a basic pH and 0.1 M HCl for an acidic pH. Afterwards, each sample was made up to a final concentration of 12.5 mg/ml Er leaf extract and used to determine the optimal pH for the synthesis of Er-AgNPs. Fig. 2b shows the UV–vis spectra obtained at various pH values. The acidic pH (from 3 to 5.8) resulted in no colour change, and the absence of the SPR peaks further confirmed that low pH values did not lead to the synthesis of AgNPs. In contrast, at neutral pH (7.0), a band with a maximum absorption peak was observed at 412 nm, which implied the formation of Er-AgNPs. Increasing the pH from 7 to 11 increased the absorption intensity, which can be interpreted as an increase in the nucleation rate and concentration of Er-AgNPs [56]. This could also imply that the high pH of the medium improved the reducing and stabilizing capacity of the biomolecules present in the Er leaf extract. Therefore, the most favourable synthesis of Er-AgNPs occurred at pH 11. The absence of definite SPR peaks at acidic pH values could be related to the electrostatic repulsion of anions present in the solution. This finding is in agreement with the literature that established the importance of the alkaline medium in the synthesis of AgNPs [12,55,57,58].

3.2.3. *Effects of the $AgNO_3$ concentration on Er-AgNPs biosynthesis*

The concentration of the $AgNO_3$ precursor is a critical parameter in the formation of AgNPs which directly impacts the size, shape, optical properties, stability, and yield of the AgNPs. Therefore, it is essential to optimize this parameter based on the desired properties and application of the NPs to achieve controlled and reproducible results in nanomaterial synthesis [59]. Fig. 3a shows the UV–vis spectra of Er-AgNPs synthesized with different concentrations of $AgNO_3$. A dose-dependent increase in the SPR peak and absorption intensity (0.22–1.40) was observed in the range of selected concentrations. The SPR peak shifted from 406 nm at 0.5 mM to 416 nm at 5 mM $AgNO_3$. Synthesis at the lowest $AgNO_3$ concentration (0.5 mM) revealed an asymmetric shape, which indicated that the formation of Er-AgNPs was not favourable at this concentration.

The optical properties of the Er-AgNPs were further characterized by measuring the full width at half maximum (FWHM). FWHM is commonly used to assess the broadness or sharpness and size of spectral peaks in UV–visible spectroscopic data. A smaller FWHM value indicates a narrower size distribution and sharper spectral peak, whereas a higher FWHM value signifies broader size distributions, wider spectral peaks, and less uniform NPs [60,61]. In this study, an increase in the $AgNO_3$ concentration resulted in a corresponding increase in the FWHM, which might be indicative of larger Er-AgNPs (Table S1). The narrowest absorption band, determined by the FWHM, was observed at 2 mM. Therefore, 2 mM $AgNO_3$ (characterized by an SPR peak at 408 nm and an absorbance intensity of 0.97) was considered the optimum concentration of $AgNO_3$ required for the reaction. Studies by Hashemi et al. [3] and Liaqat et al. [20] demonstrated that 0.5 mM $AgNO_3$ is not sufficient

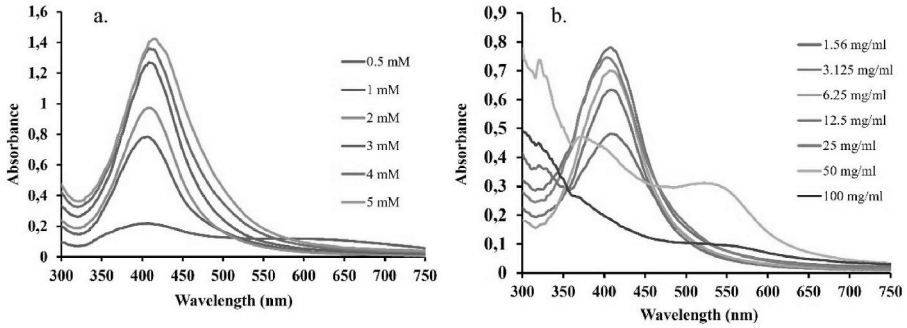

Fig. 3. UV–vis spectra showing the effects of varying (a) $AgNO_3$ concentrations and (b) Er concentrations in the leaf extracts.

for the synthesis of AgNPs. Other studies have shown that increasing the concentration of $AgNO_3$ can lead to a direct increase in the size of the AgNPs produced [59,62,63].

3.2.4. Effects of Er leaf extract concentration on Er-AgNPs biosynthesis

Various concentrations of Er leaf extracts (1.56–100 mg/ml) were used to evaluate the effects of the extract concentration on the synthesis of Er-AgNPs. The UV–vis spectra of the Er-AgNPs synthesized with various extract concentrations are shown in Fig. 3b. The lowest concentration of extract (1.56 mg/ml) had an SPR peak at 408 nm and an absorbance intensity of 0.48. Furthermore, upon increasing the concentration of Er leaf extract (up to 12.5 mg/ml), the absorbance intensity increased without a significant change in the SPR peak. However, a further increase in the extract concentration was characterized by a drastic reduction in the absorbance intensity and a broadening of the SPR peaks. The broadening and asymmetrical characteristics of the peaks became more obvious above 50 mg/ml. This finding implied that aggregation of AgNPs might be inevitable at Er concentrations greater than 12.5 mg/ml. Compared with higher concentrations, 6.25 mg/ml displayed the lowest FWHM absorbance peaks (Table S1), indicative of a desirable and smaller particle size distribution. Therefore, the optimum concentration of Er leaf extract required for the synthesis of Er-AgNPs was 6.25 mg/ml. An increase in extract concentration can increase the production of AgNPs by providing more reducing agents, thereby leading to a faster and more efficient reduction of Ag^+. However, it has been reported that high concentrations of extract can lead to the presence of excess reducing agents, which can potentially result in secondary reduction on the surface of the preformed nuclei and consequential aggregation of NPs [52,64,65].

3.2.5. Effects of Er leaf extract and silver nitrate ratio on the reaction

Various aqueous Er leaf extracts and $AgNO_3$ (v/v) were used to determine the effects of different reaction ratios on the synthesized Er-AgNPs. As shown in Fig. 4, the absence of a characteristic SPR peak was observed at the lowest reaction volume of the $AgNO_3$ solution (Fig. 4a), indicating that Er-AgNPs were not formed under these conditions. An increase in the volume of $AgNO_3$ had an impact on the size and shape of the resulting NPs. This occurred because an increase in the volume of $AgNO_3$ solution was directly proportional to an increase in the peak intensity (Fig. 4b), indicating that more Er-AgNPs were produced. Overall, a maximum absorbance spectrum at 414 nm (Fig. 4b) at a ratio of 1:9 (v/v) was obtained as the optimal reaction ratio, and the amount of Er-AgNPs produced due to the reduction in Ag^+ ions was determined from the absorbance. These findings are consistent with those reported in the literature, where the optimal condition for the synthesis of AgNPs from aqueous extracts of *Acacia cyanophylla* and *Cedrela toona* was a 1:9 (v/v) ratio of plant extract to $AgNO_3$ [66,67].

3.2.6. Effect of reaction time

The influence of reaction time was investigated by periodically examining the synthesis of Er-AgNPsat various time intervals. A visible colour change was observed almost immediately after the initiation of the reaction between the leaf extract and the $AgNO_3$ solution under the optimized conditions. The hue and absorbance intensity steadily increased as the reaction continued, reaching its highest peak after 4 h, where a sharper SPR band at approximately 408 nm was observed at an absorbance intensity of 1.85 (Fig. 5a and b). A further increase in the reaction time from 4 h to 8 h led to a noticeable decrease in the absorbance intensity (Fig. 5a and b). The latter indicated possible aggregation of the AgNPs [68,69], leading to a decrease in the concentration of

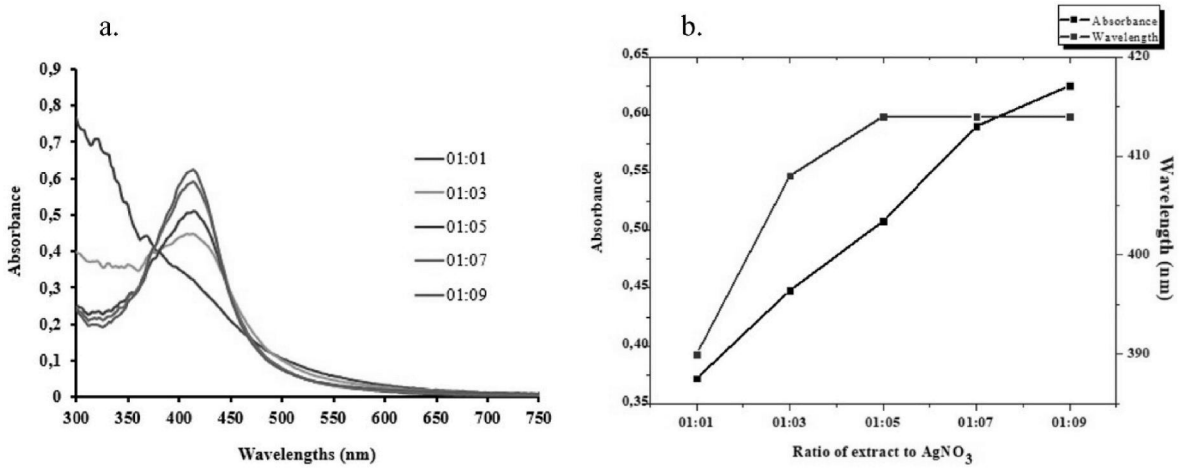

Fig. 4. Effect of the ratio of Er leaf extract to $AgNO_3$ volume in the reaction mixture. The figures show (a) the UV–vis spectra of the reaction mixture and (b) a plot of the changes in the wavelength and maximum absorbance of the reaction mixture.

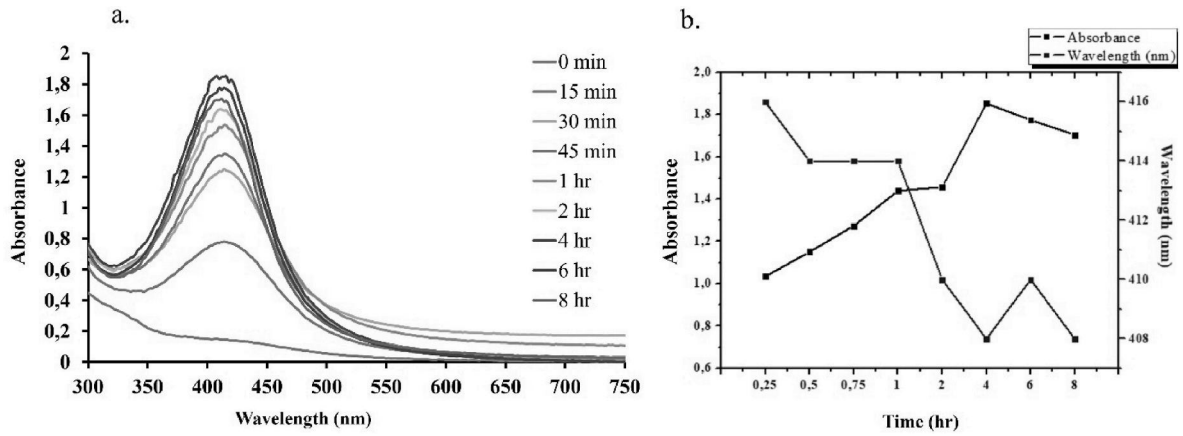

Fig. 5. UV–vis spectra of Er-AgNPs synthesized as a function of time. The figures show (a) the time-dependent UV–vis spectra for the reaction solution and (b) the plot of changes in the wavelength corresponding to the peak absorbance during synthesis.

Er-AgNPs. Therefore, the optimum time for Er-AgNPs was 4 h. The increase in absorbance intensity with time is due to an increased yield of Er-AgNPs formed from the reduction of Ag^+ ions and biomolecules in the Er leaf extract [21,32]. A similar conclusion was drawn from studies which synthesized AgNPs from aqueous extracts of *Sambucus ebulus* [3] and *Cedrela toona* leaves [67]. These studies reported that the intensity of the absorption peak increased with increasing reaction time up to 4 h.

3.3. Proposed mechanisms of action through which Ehretia rigida leaf phytochemicals facilitate the reduction and stabilization of Er-AgNPs

Based on the results obtained above, the mechanism of silver nanoparticles using Er rigida leaf aqueous extract was proposed as follows. The phytochemicals present in the extract, including phenolic acids and flavonoids, likely play a crucial role in the reduction and stabilization processes. These compounds contain hydroxyl (-OH) or carboxyl (-COOH) functional groups, which are believed to undergo deprotonation under the initial reaction conditions. The deprotonation process generates negatively charged species that exhibit enhanced reactivity and effectively interact with Ag^+ to facilitate their reduction to Ag^0 [70]. Following the reduction, atomic nuclei cluster together, initiating the nucleation and growth of AgNPs. As the NPs grow and approach their maximum size, their increasing hydrophobicity appears to attract capping agents from the extract to their surface. These capping agents likely stabilize the surface energy, preventing further aggregation and ensuring the colloidal stability of the NPs. An overview of this mechanism is presented in Equation I – V below, offering an insight into the stepwise formation and stabilization of Er-AgNPs.

Step 1: Activation of phytochemicals.

Increasing the pH of Er leaf extract facilitates deprotonation of functional groups, enhancing their ability to act as electron donor for reduction and stabilization of NPs.

$$C_{15}H_{10}O_7 \xrightarrow{NaOH} C_{15}H_9O_7^-Na^+ + H_2O \quad (I)$$

Step 2: Dissociation of $AgNO_3$ in aqueous medium.

$$AgNO_3 \rightarrow Ag^+ + NO_3^- \quad (II)$$

Step 3: Deprotonated phytochemicals in equation (I) will act as reducing agents for Ag^+ in equation (II).

$$C_{15}H_9O_7^-Na^+ + Ag^+ + NO_3^- \rightarrow C_{15}H_9O_7Ag + NaNO_3$$

$$C_{15}H_9O_7Ag \rightarrow C_{15}H_9O_7^- + Ag^+ \quad (III)$$

Step 4: Reduction of silver ion in equation (III) to zerovalent silver (AgNPs).

$$Ag^+ + e^- \rightarrow Ag^0\ (AgNPs) \quad (IV)$$

The Ag^0 formed in equation (IV) collides and sticks together due to attractive forces, forming small clusters which results in the nucleation and growth of the synthesized NPs.

Step 5: The oxidized phytochemicals will bind to the surface of the AgNPs, stabilizing them and preventing aggregation.

$$AgNPs + C_{15}H_9O_7^- \rightarrow C_{15}H_9O_7 - AgNPs \quad (V)$$

Overall, equations (I) - (V) is represented as follows;

$$AgNO_3 + C_{15}H_9O_7Na \rightarrow AgNPs + C_{15}H_9O_7 + NaNO_3$$

In summary, an illustration of the above mechanism is provided in the Scheme 1 below:

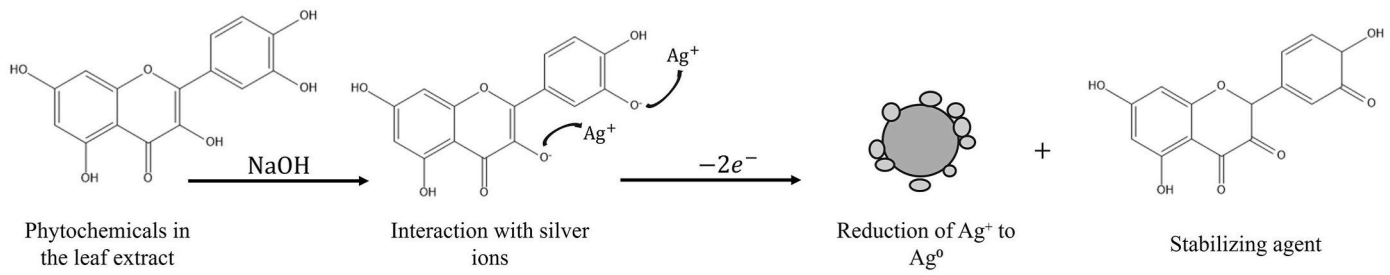

Scheme 1. Proposed mechanism of Er-AgNPs synthesis.

3.4. Characterization of Er-AgNPs

Er-AgNPs were characterized using several techniques, such as DLS, HR–TEM, selected area electron diffraction (SAED), and energy-dispersive X–ray spectroscopy (EDX), which were used to characterize the Er-AgNPs.

3.4.1. DLS analysis

DLS is a rapid and non-invasive tool that uses Brownian motion to estimate the particle size distribution and ζ potential in a suspension. It is an essential characterization step prior to any application of charged particles [71]. In this study, the hydrodynamic size, PDI, and ζ potential of Er-AgNPs were evaluated. The average size of the Er-AgNPs was 88.058 ± 8.24 nm (Fig. 6a), and the PDI was 0.36 ± 0.03, which indicated that the biosynthesized Er-AgNPs were monodispersed in terms of size distribution. The ζ potential was −25.43 ± 1.04 mV (Fig. 6b), indicating the influence of strong repulsive forces between the Er-AgNPs in suspension, which prevented their aggregation in solution. These findings are in agreement with other studies where negative values of ζ potential were obtained for green synthesized AgNPs [72,73]. A previous study also established that ζ potential values within the range of ±30 mV were moderately stable in solution [74]. Therefore, it can be concluded that AgNPs stabilized with phytochemicals from the Er leaf extract forms a stable suspension.

3.4.2. FTIR spectroscopy of Er leaf extract and Er-AgNPs

FTIR spectroscopy revealed the organic and inorganic functional groups present in the Er leaf extract and the Er-AgNPs. Fig. 7 shows an overlay of the spectra of the leaf extract and Er-AgNPs Peaks are visible at approximately 3440, 2090, 1638, and 683 cm^{-1} for the leaf extract. The broad signal at 3440 cm^{-1} corresponds to the stretching vibrations of bound and non-bonded O–H groups from alcohols or phenols. The peak at approximately 2090 cm-1 can be assigned to C ≡C stretching. The sharp peak at 1638 cm^{-1} can be assigned to N–H, corresponding to the presence of amino acids or amide I. The peak at approximately 683 cm^{-1} can be assigned to the C–Cl bending vibrations of aromatic rings. The FTIR spectrum of the Er-AgNPs shifted from 3440 cm^{-1} to 3290 cm^{-1} for O–H, and from 1638 cm^{-1} to 1623 cm^{-1} for C═O. These shifts, and the loss of peaks at approximately 2090 and 683 cm^{-1} indicated that certain functional groups of biomolecules which could include phenolic compounds, flavonoids, proteins, and saponins present in the aqueous extract were directly involved in the reduction of Ag^{+} ions and the stabilization of the synthesized NPs. These findings are in agreement with the literature, where similar functional groups have been reported to play key roles in the synthesis of plant extract-based NPs [75–77].

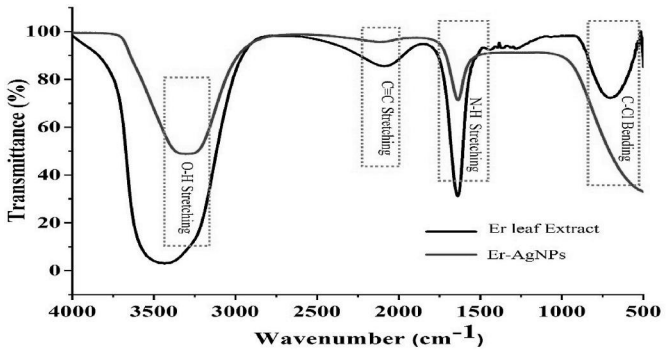

Fig. 7. FTIR spectra of Er leaf aqueous extract and the synthesized Er-AgNPs.

3.4.3. HR–TEM, SAED and EDX

The morphology and core size of the Er-AgNPs were further analysed using HR–TEM. Fig. 8a shows that the phytochemical reduction of Ag^{+} ions resulted in the formation of spherical Er-AgNPs. The core sizes of the Er-AgNPs ranged from 5 to 18 nm (Fig. 8b), with an average size distribution of 10.08 ± 2.49 nm. This size was smaller than those obtained by DLS. This is because HR–TEM measures the core size, whereas DLS measures the hydrodynamic diameter in the hydrated state, including the core size and any associated solvation layers and coatings, leading to variations in size [78]. The crystallographic properties of the Er-AgNPs, as determined from the SAED pattern, are presented in Fig. 8c. The micrograph showing concentric rings with intermittent dots confirms the face-centred crystalline nature of the Er-AgNPs. Furthermore, EDX analysis, which reveals the elemental composition of the NPs, revealed an optical adsorption peak at 3 keV, which further confirmed that the Er-AgNPs contained Ag (Fig. 8d). Similar results were previously reported for leaf extract-synthesized AgNPs, which presented an optical adsorption peak in the range of 2–4 keV [46,79]. The presence of strong adsorption peaks of copper and carbon was due to the TEM grid that was used to support the sample, whereas the presence of oxygen peaks was attributed to the capping biomolecules.

3.5. Quantitative phytochemical screening and total antioxidant capacity

3.5.1. Phytochemical screening: TPC and TFC analysis

The TPC of both the Er leaf extract and Er-AgNPs were measured as a function of the gallic acid standard, expressed as mg gallic acid equivalents (GAE) per gram of sample in dry weight (mg GAE/g). The TPC of Er-AgNPs was equivalent to 58.28 ± 1.02 mg GAE/g, and that of the Er leaf extract was 189.03 ± 6.35 mg GAE/g (Table 1). In the case of TFC,

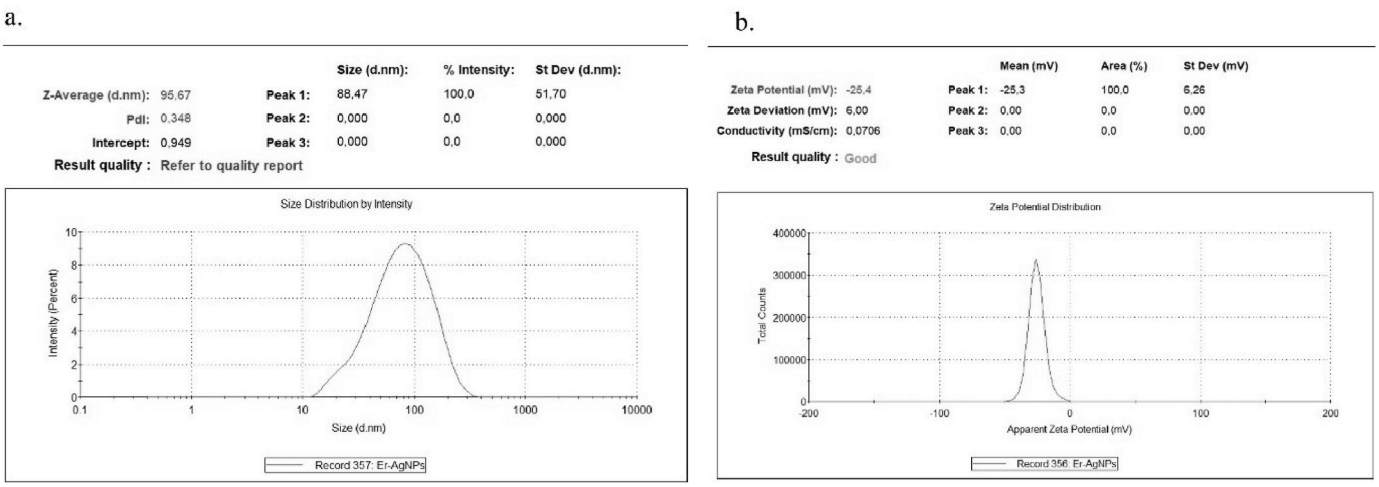

Fig. 6. DLS analyses of Er-AgNPs. (a) Particle hydrodynamic size distribution and (b) ζ potential measurement of the Er-AgNPs.

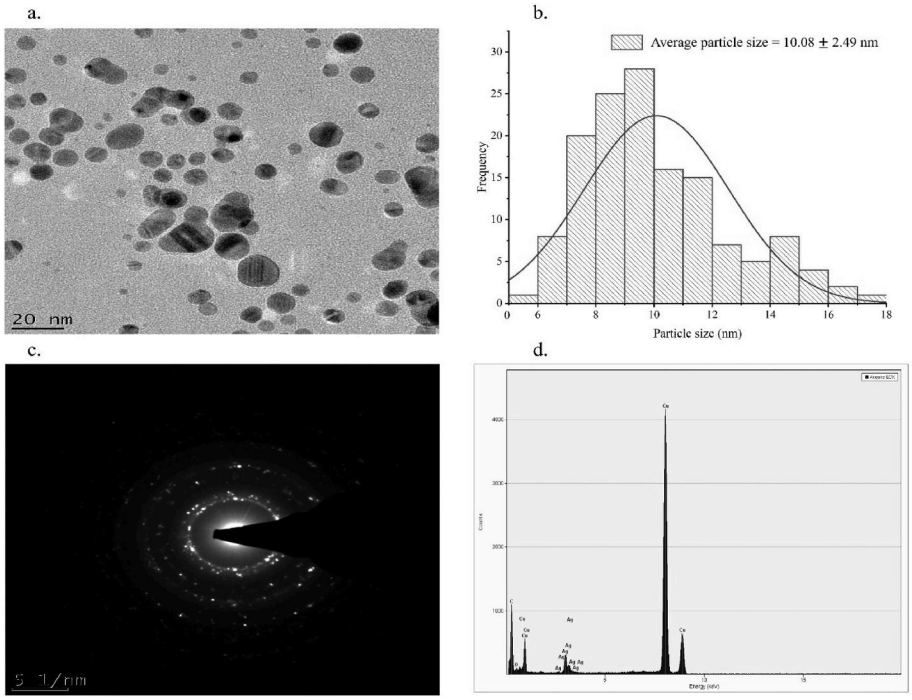

Fig. 8. HR–TEM analysis of Er-AgNPs. (a) TEM images of Er-AgNPs at the 20 nm scale; (b) size distribution of the Er-AgNPs calculated from the TEM micrograph; (c) SAED pattern; and (d) EDX spectrum for elemental composition analysis.

quercetin was used as a standard and expressed as mg of quercetin equivalents (QE) per gram of sample in dry weight (mg QE/g). The TFC of Er-AgNPs was 294.54 ± 8.50 mg QE/g, and that of the Er leaf extract was 179.17 ± 2.42 mg QE/g. The results revealed an abundance of flavonoids rather than phenolics in the Er-AgNPs extract compared with the Er leaf extract. This indicates that flavonoids may have played a more significant role in synthesis of the NPs compared to non-flavonoid compounds. The low amount of phenolic contents in Er-AgNPs could be attributed to the alteration or loss of these compounds during synthesis since this process involves exposure to high temperatures and pH changes [80]. Therefore, further optimization of these parameters may enhance the retention of antioxidant properties. Flavonoids possess unique chemical properties and a high affinity for metallic ions [81]. Dzoyem et al. [82] studied the antioxidant activity of leaf acetone extracts of twelve plants used traditionally to alleviate pain and inflammation in South Africa. They reported that *E. rigida* (1 mg/ml) presented a TPC of 103.28 ± 4.26 mg GAE/g and a TFC of 6.34 ± 2.77 mg QE/g. Phull et al. [83] synthesized AgNPs from the rhizome of *Bergenia ciliate* and reported increased TPC and TFC values compared with those of the leaf extract. Saad et al. [84] fabricated AgNPs from the peel of pomegranate and watermelon peel extracts and reported that the TPC of the AgNPs was significantly greater (10–75 %) than that of their respective extracts.

3.5.2. Total antioxidant capacity

The antioxidant activity of the Er leaf extract and Er-AgNPs was examined using DPPH, ABTS, and FRAP radical scavenging assays. As shown in Fig. 9a, the Er leaf extract and Er-AgNPs exhibited dose-dependent increases in the radical scavenging activities of DPPH. The percentage of inhibition at the highest concentration (100 μg/ml) of the Er leaf extract was 58.77 ± 2.31 %, whereas the same concentration of Er-AgNPs resulted in a scavenging yield of 34.35 ± 1.44 %. These findings implied that the leaf extracts presented significantly greater ($p < 0.005$) scavenging properties than the Er-AgNPs extracts did. However, the antioxidant activity of the extract was lower than that of the standard AA, which showed an inhibition percentage of 91.91 ± 4.54 % at 100 μg/ml.

As shown in Fig. 9b, all the tested samples exhibited dose-dependent scavenging activities against the ABTS radical. The Er leaf extract significantly ($p < 0.001$) inhibited the growth, with percentages ranging from 8.79 ± 1.78 to 93.79 ± 3.39 % across a concentration range of 6.25–100 μg/ml, whereas the Er-AgNPs concentration ranged between 6.77 ± 2.06 and 60.65 ± 4.75 %. The AA standard revealed higher scavenging activities than the ABTS standard did, ranging from 28.69 ± 2.25 to 99.93 ± 1.11 %. Non-etheless, Er leaf extract at 100 μg/ml had equivalent scavenging activity to that of AA (93.79 ± 3.39 vs 99 ± 1.11 %).

The FRAP assay was used to determine the ability of the samples to reduce ferric (III) iron to ferrous iron, expressed as μM Fe (II) equivalents. As shown in Fig. 9c, the FRAP values of all the samples increased in a dose-dependent manner, with significant differences ($p < 0.001$) observed between them. The FRAP value of the Er leaf extract ranged from 40.82 ± 5.10 to 449.45 ± 41.38 μM Fe (II) equivalent across a concentration range of 12.5–400 μg/ml. In comparison, Er-AgNPs presented FRAP values ranging from 37.93 ± 4.85 and 355.14 ± 25.56 μM Fe (II) equivalent, whereas the AA standard presented higher scavenging activity, with values ranging from 80.82 ± 7.46 to 768.47 ± 5.80 %. The FRAP assay directly estimates the amount of antioxidants in a sample by measuring their ferric-reducing activity. Overall, the results confirmed that the tested samples possessed antioxidant activity, although the activity was lower for Er-AgNPs extracts than for Er leaf extracts, which, in turn, was lower than that for AA. The greater antioxidant activity of the Er leaf extract compared to the Er-AgNPs could be attributed to the abundance of phenolic compounds in the Er leaf extract. These findings are consistent with previous reports on the total antioxidant capacities of plant extracts and their AgNPs [85,86]. In contrast, AgNPs

Table 1
TPC and TFC of Er leaf extract and Er-AgNPs.

Sample	TPC mg GAE/g	TFC mg QE/g
Leaf extract	189.03 ± 6.35	179.17 ± 2.42
Er-AgNPs	58.28 ± 1.02	294.54 ± 8.50

Data are presented as the means ± SD (n = 6).

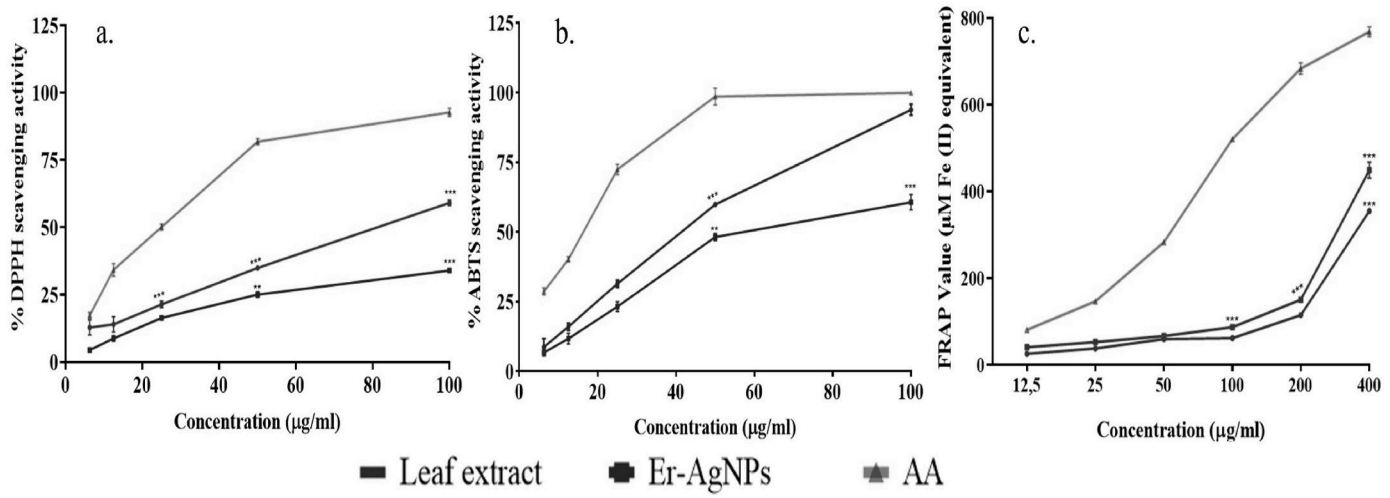

Fig. 9. Scavenging activities of Er leaf extract, Er-AgNPs, and AA at various concentrations against (a) DPPH, (b) ABTS, and (c) FRAP radicals. Each value represents the mean ± standard error of the mean (SEM) when n = 9. Data analysis was performed using one-way analysis of variance (ANOVA), followed by Bartlett's multiple comparison test, and statistical significance was indicated with $^{**}p < 0.005$ and $^{***}p < 0.001$ for comparisons between Er leaf extract and Er-AgNPs or Er leaf extract and AA.

synthesized from other extracts such as, walnut fruits (*Juglans regia*) [87], aerial parts of *Echium vulgare* and *Salvia absconditiflora* [88,89], as well as *Desmostachya bipinnata* and *Sambucus ebulus* leaf extracts [23, 90], have been shown to have higher antioxidant activities compared to their respective extracts. Non-etheless, the leaf extracts from *E. rigida* and their AgNPs could serve as valuable antioxidants for health protection against oxidative stress-related diseases.

3.6. Stability of Er-AgNPs in biological media

The colloidal stability of NPs in biological media can influence their surface charge, protein corona formation, biodistribution, bioavailability, and toxicity. Therefore, it is crucial to synthesize stable NPs that can minimize ion dissolution and retain their physicochemical properties during biological and analytical applications [31]. In the present study, the stability of the optimized Er-AgNPs in ddH_2O and culture medium at 37 °C was determined via UV–vis spectrum analysis. As indicated in Fig. 10a, Er-AgNPs were stable in ddH_2O. The Er-AgNPs placed in MHB were characterized by broadening and flattening of the absorption peaks over time (Fig. 10b); however, the resulting wavelength corresponding to the SPR peak of Er-AgNPs remained relatively the same. The observed decrease in the spectra with MHB might be due to the combination of changes in size distribution and aggregation of NPs in the culture medium [28]. The culture medium contains proteins, starch, casein hydrolysate, peptone, meat/yeast extracts, and salts. Some of these components support optimal growth, whereas others adsorb on the surface of the NPs, forming a corona that alters their biological identity. This corona can enhance the stability of the NPs while also altering their activity. Other components, including salts and charged proteins, can affect the stability of nanoparticles and promote the formation of clusters, lowering the total surface area and thus masking the antimicrobial efficacy of the NPs [91,92].

3.7. Antimicrobial studies

3.7.1. Agar well diffusion

An agar well diffusion assay is a preliminary method used to evaluate the antimicrobial activity of a sample, typically indicated by a clear zone around the well containing the test sample on an agar plate and the subsequent measurement of the clear zone to assess the level of antimicrobial activity. In this study, the antimicrobial activities of Er leaf extract and Er-AgNPs were screened against three Gram-positive (*S. aureus,* MRSA, and *S. pyogenes*) strains, five Gram-negative (*A. baumannii, E. coli, E. cloacae, K. pneumoniae,* and *P. aeruginosa*) bacterial strains, and one yeast (*C. albicans*) strain using an agar well diffusion assay. As shown in Fig. 11 and Table 2, no clear ZOIs were observed for any of the bacteria and fungus treated with the Er leaf extract. These findings indicated that the extract had no antimicrobial effects at the tested concentrations. In most cases, extracts are usually effective at very high concentrations. For example, methanolic leaf extracts prepared from *E. serrata* demonstrated promising antibacterial activities against all tested human pathogens (*Azospirillum lipoferum, P. aeruginosa, and S. aureus*) at 40 mg/ml [93]. Similarly, *E. laevis* Roxb extracts produced with different solvents (chloroform, methanolic, and

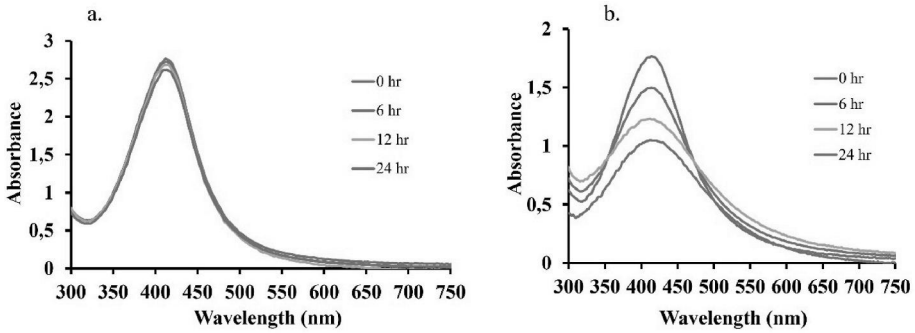

Fig. 10. Stability of the synthesized Er-AgNPs during incubation in (a) ddH_2O and (b) MHB at 37 °C. UV–vis analysis of the NPs was performed over a 24–hr period.

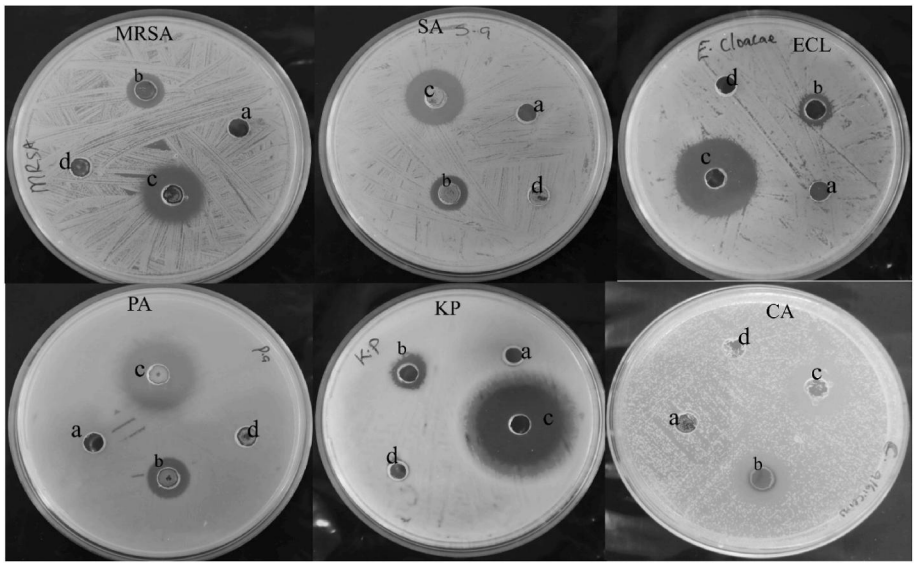

Fig. 11. Selected agar well diffusion results showing the ZOIs for the various treatments against MRSA, *S. aureus, E. cloacae, P. aeruginosa, K. pneumoniae,* and *C. albicans.* Treatments: (a) Er leaf aqueous extract, (b) Er-AgNPs, (c) ciprofloxacin/amphotericin B, and (d) MHB/PDB.

Table 2
Antimicrobial activities of Er leaf extract and Er-AgNPs were determined using agar well diffusion assay.

	Pathogens	Leaf extract	Er-AgNPs (Mean ± SD)	Ciprofloxacin/Amphotericin B (Mean ± SD)
Gram-positive	MRSA	0.00	12.33 ± 2.31	20.33 ± 3.21****
	S. aureus	0.00	11.67 ± 1.15	25.67 ± 0.58 ****
	S. pyogenes	0.00	16.33 ± 0.57	39.00 ± 1.00 ****
Gram-negative	*A. baumannii*	0.00	12.00 ± 0.00	36.67 ± 1.53 ****
	E. cloacae	0.00	12.33 ± 0.58	36.33 ± 1.53****
	E. coli	0.00	10.33 ± 0.57	38.67 ± 0.58 ****
	K. pneumoniae	0.00	15.00 ± 0.00	34.67 ± 2.52 ****
	P. aeruginosa	0.00	13.33 ± 0.58	23.67 ± 3.51****
Fungus	*C. albicans*	0.00	18.33 ± 1.57	17.33 ± 2.52

The results are displayed as the mean diameter (mm) of three independent experiments. Each value was expressed as the mean ± standard deviation. Data analysis was performed using one-way ANOVA, and the statistical significance ($p < 0.0001$) between Er-AgNPs-treated pathogens and the positive control is indicated with an asterisk (****).

water extracts) had excellent antibacterial activities against a wide range of pathogens [94]. In another study, dried leaf powder and fresh leaf paste (50–100 mg/ml) of *E. laevis* leaves extracted separately with acetone or ethyl alcohol (95 %) showed excellent antibacterial and antifungal activities against oral pathogens, particularly *S. aureus* and *Candida* spp [95].

As shown in Fig. 11 and Table 2, Er-AgNPs effectively inhibited both Gram-positive and Gram-negative bacteria, which indicated that the antibacterial activity of Er-AgNPs was not affected by differences in bacterial cell walls. These results are in agreement with those of previous studies [39,74], whereas other reports have established that Gram-negative bacteria are more susceptible to green synthesized AgNPs [9,72,75]. Compared with the Er leaf extract and Er-AgNPs, the positive control, ciprofloxacin, had greater antibacterial activity. The susceptibility of *C. albicans* to Er-AgNPs was comparable to that of amphotericin B, with ZOIs of 18.33 ± 1.57 and 17.33 ± 2.52 mm, respectively. This observation is consistent with the study by Malathi et al. [96], who reported a ZOI value of 18 mm for *C. albicans* treated with amphotericin B, whereas values ranging from 20 ± 0.75 to 22 ± 0.43 were obtained for those exposed to AgNPs. The enhanced antimicrobial activity of the Er-AgNPs in this study could be attributed to better diffusion and penetration of the small Er-AgNPs into the microbes than the leaf extracts [97]. Additionally, the observed antimicrobial activities of Er-AgNPs may also result from the adhesion of the AgNPs onto the surface of the cell wall and membrane, their penetration into the cell, and subsequent damage to intracellular structures and biomolecules such as DNA and RNA [2,98].

3.7.2. Minimum inhibitory and minimum bactericidal/fungicidal concentrations

To further validate the antimicrobial effects observed by agar well diffusion tests, further tests, such as MIC and MBC/MFC, are essential to provide more detailed information about the antimicrobial properties of a test sample. These tests determine the lowest concentration that inhibits growth (MIC) and the lowest concentration that kills bacteria or fungi (MBC/MFC) [99]. In this study, the MICs of Er-AgNPs and ciprofloxacin/amphotericin B were determined against the nine tested pathogens. Er-AgNPs inhibited all the pathogens at concentrations ranging from 200 to 800 μg/ml (Table 3). Among them, MRSA and *C. albicans* were observed to require the highest inhibitory concentration of 800 μg/ml, while the MICs of *A. baumannii, E. coli,* and *S. pyogenes* were 400 μg/ml. The growth of *S. aureus, K. pneumoniae, E. cloacae,* and *P. aeruginosa* was inhibited the least at a concentration of 200 μg/ml, suggesting increased sensitivity to Er-AgNPs. Ciprofloxacin had an MIC range of 0.078–1.25 μg/ml against bacteria, whereas amphotericin B had an MIC value of 2.5 μg/ml against *C. albicans.*

The MBC/MFC of the treatments was determined by re-culturing the diluted MIC cultures on fresh agar plates. As shown in Table 3, *S aureus* and *E. coli* had the lowest bactericidal concentrations, requiring 200 and 400 μg/ml, respectively. All other tested bacteria had MBCs ≥800 μg/ml. In line with the present findings, AgNPs synthesized using an aqueous extract of *Ducrosia flabellifolia* had potent anti–ESKAPE activity,

Table 3
MIC and MBC values of Er-AgNPs and known antibiotics against selected bacterial strains and fungus.

Pathogens	Er-AgNPs		Ciprofloxacin/Amphotericin B	
	MIC (μg/ml)	MBC (μg/ml)	MIC (μg/ml)	MBC (μg/ml)
MRSA	800	800	0.313	0.650
S. aureus	200	200	0.313	0.625
S. pyogenes	400	>800	0.625	2.500
A. baumannii	400	>800	0.625	2.500
E. cloacae	200	>800	0.078	0.625
E. coli	400	400	0.156	0.156
K. pneumoniae	200	>800	0.078	1.250
P. aeruginosa	200	>800	1.250	2.500
C. albicans	800	>800	1.250	2.500

Notes: Results are expressed as the means of three independent experiments.

with MIC and MBC values ranging from 78 to 312 and 312–625 μg/ml, respectively [100]. AgNPs synthesized using *Salvia africana-Lutea* (SAL) had MIC values of 187.5 and 375 μg/ml against *S. epidermidis* and *P. aeruginosa*, respectively, whereas *Sutherlandia frutescens* (SF) had a higher MIC value of 750 μg/ml for both pathogens [28]. Other studies have also demonstrated that AgNPs from various leaf aqueous extracts presented significantly increased antimicrobial activities against *S. aureus, E. coli, K. pneumoniae, P. aeruginosa, Citrobacter freundi, Achromobacter xylosoxidans*, *Morganella morganii*, *K. oxytoca*, *Salmonella enteritidis,* and *Candida* species [23,101–103]. Therefore, the Er-AgNPs synthesized in this study have potential as broad-spectrum antimicrobial agents.

4. Conclusion

In this study, Er-AgNPs was successfully synthesized using Er leaf aqueous extract. The green synthesis approach employed here offers a rapid, cost-effective, and efficient method for fabricating AgNPs. The Er-AgNPs were synthesized under the optimal conditions of pH 11, 50 °C, 6.25 mg/ml Er leaf extract and 2 mM $AgNO_3$ at a 1:9 ratio, with a reaction time of 4 h. The resulting Er-AgNPs were stable, spherical, and crystalline, with an average size of 10.08 ± 2.49 nm. FTIR confirmed the direct involvement of biomolecules from phenolic compounds, flavonoids, proteins, and saponins in the reduction of Ag^+ and stabilization of the synthesized NPs. The Er leaf extract exhibited stronger antioxidant activity than the Er-AgNPs. In contrast, the Er-AgNPs demonstrated enhanced antimicrobial activity against a wide range of pathogenic bacteria and fungus. Overall, this research underscores the potential of Er leaf extract as a valuable reducing and capping agent for the green synthesis of AgNPs, thus offering a sustainable and eco-friendly alternative to conventional chemical and physical synthesis methods.

CRediT authorship contribution statement

Samson O. Oselusi: Writing – original draft, Methodology, Formal analysis, Conceptualization. **Nicole R.S. Sibuyi:** Writing – review & editing, Supervision. **Mervin Meyer:** Writing – review & editing. **Samantha Meyer:** Writing – review & editing. **Abram M. Madiehe:** Writing – review & editing, Supervision, Conceptualization.

Data availability statement

Data will be made available on request.

Declaration of competing interest

The authors declare that they have no known competing financial interests or personal relationships that could have appeared to influence the work reported in this paper.

Acknowledgments

The author SOO extends his appreciation to the South African National Research Foundation (NRF) for his Doctoral Scholarship Award (Reference: MND210616612113). The authors also acknowledge the DSI/Mintek NIC for financial support.

Appendix A. Supplementary data

Supplementary data to this article can be found online at https://doi.org/10.1016/j.mtsust.2024.101059.

Data availability

Data will be made available on request.

References

[1] E. Ajayi, A. Afolayan, Green synthesis, characterization and biological activities of silver nanoparticles from alkalinized Cymbopogon citratus Stapf, Adv. Nat. Sci. Nanosci. Nanotechnol. 8 (1) (2017) 015017.
[2] I. Khan, K. Saeed, I. Khan, Nanoparticles: properties, applications and toxicities, Arab. J. Chem. 12 (7) (2019) 908–931.
[3] Z. Hashemi, et al., Sustainable green synthesis of silver nanoparticles using Sambucus ebulus phenolic extract (AgNPs@ SEE): optimization and assessment of photocatalytic degradation of methyl orange and their in vitro antibacterial and anticancer activity, Arab. J. Chem. 15 (1) (2022) 103525.
[4] A. Sharma, et al., Nanomaterials and nanotechnology: a comprehensive study of synthesis, characterization and multifaceted applications, Biochem. Cell. Arch. 23 (2023) 1641–1647.
[5] W.A. Shaikh, et al., A review of the phytochemical mediated synthesis of AgNP (silver nanoparticle): the wonder particle of the past decade, Appl. Nanosci. 11 (11) (2021) 2625–2660.
[6] S. Agrawal, et al., Silver nanoparticles and its potential applications: a review, J. Pharmacogn. Phytochem. 7 (2) (2018) 930–937.
[7] K. Ganguly, et al., Silver nanoparticles for wastewater treatment, in: Aquananotechnology, Elsevier, 2021, pp. 385–401.
[8] P. Verma, S.K. Maheshwari, Applications of Silver nanoparticles in diverse sectors, Int. J. Nano Dimens. (IJND) 10 (1) (2019) 18–36.
[9] M. Zahoor, et al., A review on silver nanoparticles: classification, various methods of synthesis, and their potential roles in biomedical applications and water treatment, Water 13 (16) (2021) 2216.
[10] A. Meher, et al., Silver nanoparticle for biomedical applications: a review, Hybrid Advances (2024) 100184.
[11] A.I. Osman, et al., Synthesis of green nanoparticles for energy, biomedical, environmental, agricultural, and food applications: a review, Environ. Chem. Lett. 22 (2) (2024) 841–887.
[12] M. Aslam, et al., Phyto-extract-mediated synthesis of silver nanoparticles using aqueous extract of Sanvitalia procumbens, and characterization, optimization and photocatalytic degradation of azo dyes Orange G and Direct Blue-15, Molecules 26 (20) (2021) 6144.
[13] A. Nyabadza, et al., A review of physical, chemical and biological synthesis methods of bimetallic nanoparticles and applications in sensing, water treatment, biomedicine, catalysis and hydrogen storage, Adv. Colloid Interface Sci. 321 (2023) 103010.
[14] J. Sukweenadhi, et al., Scale-up of green synthesis and characterization of silver nanoparticles using ethanol extract of Plantago major L. leaf and its antibacterial potential, S. Afr. J. Chem. Eng. 38 (1) (2021) 1–8.
[15] S.O. Oselusi, et al., Phytonanotherapeutic applications of plant extract-synthesized silver nanoparticles in wound healing—a prospective overview, BioNanoScience 14 (2024) 3455–3475.
[16] X.-F. Zhang, et al., Silver nanoparticles: synthesis, characterization, properties, applications, and therapeutic approaches, Int. J. Mol. Sci. 17 (9) (2016) 1534.
[17] L. Castillo-Henríquez, et al., Green synthesis of gold and silver nanoparticles from plant extracts and their possible applications as antimicrobial agents in the agricultural area, Nanomaterials 10 (9) (2020) 1763.
[18] E.A. Flores-Contreras, et al., Agricultural waste as a sustainable source for nanoparticle synthesis and their antimicrobial properties for food preservation, Frontiers in Nanotechnology 6 (2024) 1346069.
[19] E.K. Kocazorbaz, Green Synthesis, optimization, and characterization of silver nanoparticles from Euphorbia rigida Leaf Extract and Investigation of their Antimicrobal activities, Bilecik Şeyh Edebali Üniversitesi Fen Bilimleri Dergisi 8 (2) (2021) 512–522.
[20] N. Liaqat, et al., Green synthesized silver nanoparticles: optimization, characterization, antimicrobial activity, and cytotoxicity study by hemolysis assay, Front. Chem. 10 (2022) 952006.
[21] S.N.A. Mat Yusuf, et al., Optimization of biogenic synthesis of silver nanoparticles from flavonoid-rich Clinacanthus nutans leaf and stem aqueous extracts, R. Soc. Open Sci. 7 (7) (2020) 200065.

[22] K. Okaiyeto, et al., Phytofabrication of silver/silver chloride nanoparticles using aqueous leaf extract of Oedera genistifolia: characterization and antibacterial potential, Molecules 24 (23) (2019) 4382.
[23] T. Karan, et al., Green synthesis of silver nanoparticles using Sambucus ebulus leaves extract: characterization, quantitative analysis of bioactive molecules, antioxidant and antibacterial activities, J. Mol. Struct. 1296 (2024) 136836.
[24] A. Maroyi, A systematic review on biological and medicinal properties of Ehretia rigida (Thunb.) Druce (Ehretiaceae) in Southern Africa, Plant Science Today 10 (sp2) (2023) 74–82.
[25] A. Shukla, A. Kaur, A systematic review of traditional uses bioactive phytoconstituents of genus Ehretia, Asian J. Pharmaceut. Clin. Res. 11 (6) (2018) 88–100.
[26] P. Sharma, et al., Phytochemical and ethnopharmacological perspectives of Ehretia laevis, Molecules 26 (12) (2021) 3489.
[27] S.O. Oselusi, et al., Ehretia Species Phytoconstituents as Potential Lead Compounds against Klebsiella pneumoniae Carbapenemase: A Computational Approach, BioMed Research International, 2023, p. 2023.
[28] P. Dube, et al., Antibacterial activity of biogenic silver and gold nanoparticles synthesized from Salvia africana-lutea and Sutherlandia frutescens, Nanotechnology 31 (50) (2020) 505607.
[29] N.J. Deka, et al., Green synthesis and characterization of silver nanoparticles using leaves extract of Neem (Azadirachtaindica L.) and assessment of its in vitro antioxidant and antibacterial activity, Ann. Phytomed. 10 (1) (2021) 171–177.
[30] J.E. Graves, et al., Ultrasound assisted dispersal of a copper nanopowder for electroless copper activation, Ultrason. Sonochem. 29 (2016) 428–438.
[31] Y.L. Balachandran, et al., Differently environment stable bio-silver nanoparticles: study on their optical enhancing and antibacterial properties, PLoS One 8 (10) (2013) e77043.
[32] G. Arya, et al., Green synthesis of silver nanoparticles using Prosopis juliflora bark extract: reaction optimization, antimicrobial and catalytic activities, Artif. Cell Nanomed. Biotechnol. 46 (5) (2018) 985–993.
[33] G. Singh, et al., Evaluation of phenolic content variability along with antioxidant, antimicrobial, and cytotoxic potential of selected traditional medicinal plants from India, Front. Plant Sci. 7 (2016) 407.
[34] S. Maungchanburee, et al., Study of antioxidant activities, total phenolic content and total flavonoid content of the extracts of Monochoria vaginalis and Cissus repens Lamk. using different solvents, J. Pharmaceut. Sci. Res. 12 (3) (2020) 356–359.
[35] A.I. Daniel, et al., Nelsonia canescens (Acanthaceae) aqueous extract and partitioned fractions ameliorates type-2 diabetes in alloxan-induced diabetic rats, Future Journal of Pharmaceutical Sciences 8 (1) (2022) 53.
[36] N.S. Rajurkar, S. Hande, Estimation of phytochemical content and antioxidant activity of some selected traditional Indian medicinal plants, Indian J. Pharmaceut. Sci. 73 (2) (2011) 146.
[37] A. Elbermawi, et al., In vitro antidiabetic, antioxidant, and prebiotic activities of the chemical compounds isolated from Guizotia abyssinica, Antioxidants 11 (12) (2022) 2482.
[38] M. Balouiri, M. Sadiki, S.K. Ibnsouda, Methods for in vitro evaluating antimicrobial activity: a review, Journal of Pharmaceutical Analysis 6 (2) (2016) 71–79.
[39] Y.Y. Loo, et al., In vitro antimicrobial activity of green synthesized silver nanoparticles against selected gram-negative foodborne pathogens, Front. Microbiol. 9 (2018) 1555.
[40] M. Mackeen, et al., Antimicrobial and cytotoxic properties of some Malaysian traditional vegetables (ulam), Int. J. Pharmacogn. 35 (3) (1997) 174–178.
[41] C. Bitwell, et al., A review of modern and conventional extraction techniques and their applications for extracting phytochemicals from plants, Scientific African 19 (2023) e01585.
[42] N. Flórez, E. Conde, H. Domínguez, Microwave assisted water extraction of plant compounds, J. Chem. Technol. Biotechnol. 90 (4) (2015) 590–607.
[43] H. Azwatul, et al., Plant-based green synthesis of silver nanoparticle via chemical bonding analysis, Mater. Today: Proc. (2023) 5942.
[44] M. Gomathi, et al., Green synthesis of silver nanoparticles using Datura stramonium leaf extract and assessment of their antibacterial activity, Resource-Efficient Technologies 3 (3) (2017) 280–284.
[45] T. Karan, et al., Green synthesis of silver nanoparticles using Sambucus ebulus leaves extract: characterization, quantitative analysis of bioactive molecules, antioxidant and antibacterial activities, J. Mol. Struct. 1296 (1) (2024) 136836.
[46] K. Anandalakshmi, J. Venugobal, V. Ramasamy, Characterization of silver nanoparticles by green synthesis method using Pedalium murex leaf extract and their antibacterial activity, Appl. Nanosci. 6 (2016) 399–408.
[47] R. Kaur, et al., Effect of various synthesis parameters on the stability of size controlled green synthesis of silver nanoparticles, Nano Express 2 (2) (2021) 020005.
[48] P. Velmurugan, et al., Green synthesis of silver and gold nanoparticles using Zingiber officinale root extract and antibacterial activity of silver nanoparticles against food pathogens, Bioproc. Biosyst. Eng. 37 (10) (2014) 1935–1943.
[49] B.U. Hijazi, et al., Biosynthesis of silver nanoparticles as a reliable alternative for the catalytic degradation of organic dyes and antibacterial applications, Current Research in Green and Sustainable Chemistry 8 (2024) 100408.
[50] M. Ansari, et al., Plant mediated fabrication of silver nanoparticles, process optimization, and impact on tomato plant, Sci. Rep. 13 (1) (2023) 18048.
[51] Y.M. Jamil, et al., Optimum green synthesis, characterization, and antibacterial activity of silver nanoparticles prepared from an extract of Aloe fleurentinorum, Int. J. Chem. Eng. 2024 (1) (2024) 2804165.
[52] C. Vanlalveni, et al., Green synthesis of silver nanoparticles using plant extracts and their antimicrobial activities: a review of recent literature, RSC Adv. 11 (5) (2021) 2804–2837.
[53] A. Zuhrotun, D.J. Oktaviani, A.N. Hasanah, Biosynthesis of gold and silver nanoparticles using phytochemical compounds, Molecules 28 (7) (2023) 3240.
[54] A. Miranda, et al., pH alteration in plant-mediated green synthesis and its resultant impact on antimicrobial properties of silver nanoparticles (AgNPs), Antibiotics 11 (11) (2022) 1592.
[55] F.E.a. Meva, et al., Spectroscopic synthetic optimizations monitoring of silver nanoparticles formation from Megaphrynium macrostachyum leaf extract, Revista Brasileira de Farmacognosia 26 (2016) 640–646.
[56] N.S. Alharbi, N.S. Alsubhi, A.I. Felimban, Green synthesis of silver nanoparticles using medicinal plants: characterization and application, Journal of Radiation Research and Applied Sciences 15 (3) (2022) 109–124.
[57] A.O. Dada, et al., Silver nanoparticle synthesis by Acalypha wilkesiana extract: phytochemical screening, characterization, influence of operational parameters, and preliminary antibacterial testing, Heliyon 5 (10) (2019) e02517.
[58] B. Yaseen, et al., Detailed kinetic and mechanistic study for the preparation of silver nanoparticles by a chemical reduction method in the presence of a Neuroleptic Agent (Gabapentin) at an alkaline pH and its characterization, ACS Omega 7 (7) (2022) 5739–5750.
[59] A. Azad, et al., Factors influencing the green synthesis of metallic nanoparticles using plant extracts: a comprehensive review, Pharmaceutical Fronts 5 (3) (2023) e117–e131.
[60] J.P. Oliveira, et al., A helpful method for controlled synthesis of monodisperse gold nanoparticles through response surface modeling, Arab. J. Chem. 13 (1) (2020) 216–226.
[61] A.W. Orbaek, M.M. McHale, A.R. Barron, Synthesis and characterization of silver nanoparticles for an undergraduate laboratory, J. Chem. Educ. 92 (2) (2015) 339–344.
[62] Y. Htwe, et al., Effect of silver nitrate concentration on the production of silver nanoparticles by green method, Mater. Today: Proc. 17 (2019) 568–573.
[63] A. Sobczak-Kupiec, et al., Influence of silver nitrate concentration on the properties of silver nanoparticles, Micro & Nano Lett. 6 (8) (2011) 656–660.
[64] D. Chugh, V. Viswamalya, B. Das, Green synthesis of silver nanoparticles with algae and the importance of capping agents in the process, J. Genet. Eng. Biotechnol. 19 (1) (2021) 126.
[65] M.R. Shaik, et al., Plant-extract-assisted green synthesis of silver nanoparticles using Origanum vulgare L. extract and their microbicidal activities, Sustainability 10 (4) (2018) 913.
[66] J. Jalab, et al., Green synthesis of silver nanoparticles using aqueous extract of Acacia cyanophylla and its antibacterial activity, Heliyon 7 (9) (2021) e08033.
[67] M.A. Javed, et al., Biosynthesis and characterization of silver nanoparticles from Cedrela toona leaf extracts: an exploration into their antibacterial, anticancer, and antioxidant potential, Green Process. Synth. 13 (1) (2024) 20230248.
[68] A.O. Dada, et al., Exploring the effect of operational factors and characterization imperative to the synthesis of silver nanoparticles, in: K. Maaz (Ed.), *Silver Nanoparticles-Fabrication, Characterization and Applications*. 2018, IntechOpen, London, UK, 2018, pp. 165–184.
[69] M. Tesfaye, et al., Green synthesis of silver nanoparticles using Vernonia amygdalina plant extract and its antimicrobial activities, Heliyon 9 (6) (2023) e17356.
[70] U.O. Aigbe, A.O. Osibote, Green synthesis of metal oxide nanoparticles, and their various applications, Journal of Hazardous Materials Advances 13 (2024) 100401.
[71] Z. Jia, et al., Dynamic light scattering: a powerful tool for in situ nanoparticle sizing, Colloids and Interfaces 7 (1) (2023) 15.
[72] O. Ahmed, et al., Antimicrobial effects of gum Arabic-silver nanoparticles against oral pathogens, Bioinorgan. Chem. Appl. 2022 (1) (2022) 9602325.
[73] C. Tyavambiza, et al., The antimicrobial and anti-inflammatory effects of silver nanoparticles synthesised from Cotyledon orbiculata aqueous extract, Nanomaterials 11 (5) (2021) 1343.
[74] H. Ardani, et al., Enhancement of the stability of silver nanoparticles synthesized using aqueous extract of Diospyros discolor Willd. leaves using polyvinyl alcohol, IOP Conf. Ser. Mater. Sci. Eng. 188 (2017) 012056.
[75] M. Al-Ansari, et al., Facile and cost-effective Ag nanoparticles fabricated by lilium lancifolium leaf extract: antibacterial and antibiofilm potential, J. Cluster Sci. 30 (2019) 1081–1089.
[76] S. Veeramani, K. Shanmugam, Biosynthesis and characterization of silver nanoparticles coated with metabolites extracted from clerodendron phlomoides with its biochemical studies in liver tissue, Proceedings of Anticancer Research 7 (4) (2023) 1–19.
[77] M.M.I. Masum, et al., Biogenic synthesis of silver nanoparticles using Phyllanthus emblica fruit extract and its inhibitory action against the pathogen Acidovorax oryzae strain RS-2 of rice bacterial brown stripe, Front. Microbiol. 10 (2019) 820.
[78] T.G. Souza, V.S. Ciminelli, N.D.S. Mohallem, A comparison of TEM and DLS methods to characterize size distribution of ceramic nanoparticles, J. Phys. Conf. 733 (1) (2016) 012039.
[79] R. Vijayan, S. Joseph, B. Mathew, Green synthesis of silver nanoparticles using Nervalia zeylanica leaf extract and evaluation of their antioxidant, catalytic, and antimicrobial potentials, Part. Sci. Technol. 37 (7) (2019) 809–819.
[80] Z. Razali, J. Norrizah, S. Abdullah, Impact of temperature and pH on antioxidant activity of green silver nanoparticles fabricated from Ananas comosus peel extracts, in: IOP Conference Series: Earth and Environmental Science, IOP Publishing, 2022.

[81] T. Hou, et al., Exploring the biomedical applications of biosynthesized silver nanoparticles using Perilla frutescens flavonoid extract: antibacterial, antioxidant, and cell toxicity properties against colon cancer cells, Molecules 28 (17) (2023) 6431.
[82] J.P. Dzoyem, J.N. Eloff, Anti-inflammatory, anticholinesterase and antioxidant activity of leaf extracts of twelve plants used traditionally to alleviate pain and inflammation in South Africa, J. Ethnopharmacol. 160 (2015) 194–201.
[83] A.-R. Phull, et al., Antioxidant, cytotoxic and antimicrobial activities of green synthesized silver nanoparticles from crude extract of Bergenia ciliata, Future Journal of Pharmaceutical Sciences 2 (1) (2016) 31–36.
[84] A.M. Saad, et al., Polyphenolic extracts from pomegranate and watermelon wastes as substrate to fabricate sustainable silver nanoparticles with larvicidal effect against Spodoptera littoralis, Saudi J. Biol. Sci. 28 (10) (2021) 5674–5683.
[85] A.N.B. Salem, et al., Cytotoxic effect of nanoparticles synthesized from Salvia officinalis L. and Ricinus communis aqueous extracts against vero cell line and evaluation of their antioxidant activities, Afr. J. Biotechnol. 11 (52) (2012) 11530–11534.
[86] J.M. Geyesa, et al., Antibacterial and antioxidant potential analysis of Verbascum sinaiticum leaf extract and its synthesized silver nanoparticles, Heliyon 10 (2) (2024) e24215.
[87] S. Khorrami, et al., Selective cytotoxicity of green synthesized silver nanoparticles against the MCF-7 tumor cell line and their enhanced antioxidant and antimicrobial properties, Int. J. Nanomed. 13 (2018) 8013–8024.
[88] E.N. Gecer, R. Erenler, Biogenic synthesis of silver nanoparticles using Echium vulgare: characterisation, quantitative analysis of bioactive compounds, antioxidant activity and catalytic degradation, J. Indian Chem. Soc. 100 (5) (2023) 101003.
[89] R. Erenler, et al., Facile, efficient synthesis of silver nanoparticles using Salvia absconditiflora: assessment of their antioxidant capacity and catalytic activity, Inorg. Chem. Commun. 158 (2023) 111623.
[90] S.R. Guntur, et al., In vitro studies of the antimicrobial and free-radical scavenging potentials of silver nanoparticles biosynthesized from the extract of Desmostachya bipinnata, Anal. Chem. Insights 13 (2018) 1177390118782877.
[91] A.M. Ferreira, et al., How similar is the antibacterial activity of silver nanoparticles coated with different capping agents? RSC Adv. 13 (16) (2023) 10542–10555.
[92] G. Franci, et al., Silver nanoparticles as potential antibacterial agents, Molecules 20 (5) (2015) 8856–8874.
[93] A. Waheed, et al., The first report on the in vitro antimicrobial activities of extracts of leaves of Ehretia serrata, Saudi J. Biol. Sci. 26 (6) (2019) 1253–1261.
[94] N. Jyothirmai, B. Nagaraju, J.S. Kumar, Evaluation of anti-inflammatory and anti-bacterial activities of different solvent extracts of Ehretia laevis Roxb, J. Pharmaceut. Sci. Res. 8 (8) (2016) 715.
[95] D.K.W. Murarkar, S. Khadse, S. Mankar, Ehretia laevis leaves: potential herbal remedy for mouth microflora, Indian Journal of Traditional Knowledge 21 (2) (2022) 292–297.
[96] S. Malathi, et al., Silver nanoparticles, synthesized using Hyptis suaveolens (L) poit and their antifungal activity against Candida spp, ChemistrySelect 7 (47) (2022) e202203050.
[97] S.J. Bakht Dalir, et al., Characterization and the evaluation of antimicrobial activities of silver nanoparticles biosynthesized from Carya illinoinensis leaf extract, Heliyon 6 (3) (2020) e03624.
[98] T.C. Dakal, et al., Mechanistic basis of antimicrobial actions of silver nanoparticles, Front. Microbiol. 7 (2016) 1831.
[99] M.J. Goswami, et al., Synthesis, antimicrobial and antioxidant bioevaluation of silver nanoparticles using leaf extract of Sarcochlamys pulcherrima, Nanotechnology 5 (2024) 100063.
[100] M. Snoussi, et al., Green synthesis and characterization of silver nanoparticles from Ducrosia flabellifolia Boiss. aqueous extract: anti-quorum sensing screening and antimicrobial activities against ESKAPE pathogens, Cell. Mol. Biol. 70 (2) (2024) 88–96.
[101] N.M. Alabdallah, E. Kotb, Antimicrobial activity of green synthesized silver nanoparticles using waste leaves of hyphaene thebaica (Doum Palm), Microorganisms 11 (3) (2023) 807.
[102] G.P. Chuy, et al., Green nanoarchitectonics of silver nanoparticles for antimicrobial activity against resistant pathogens, J. Inorg. Organomet. Polym. Mater. 32 (2022) 1–10.
[103] M.M.J. Arsene, et al., Antimicrobial activity of phytofabricated silver nanoparticles using Carica papaya L. against Gram-negative bacteria, Vet. World 16 (6) (2023) 1301.